Supplement of Atmos. Chem. Phys., 21, 12809–12833, 2021
https://doi.org/10.5194/acp-21-12809-2021-supplement
© Author(s) 2021. CC BY 4.0 License.

Atmospheric Chemistry and Physics
Open Access
EGU

Supplement of

Source-specific light absorption by carbonaceous components in the complex aerosol matrix from yearly filter-based measurements

Vaios Moschos et al.

Correspondence to: Imad El Haddad (imad.el-haddad@psi.ch)

The copyright of individual parts of the supplement might differ from the article licence.

SUPPORTING TEXT

S1. Filter sampling

In total, 245 PM_{10} filters from Magadino (Jan '13 – Sep '14) and Zurich (Jan '13 – Dec '13), and 65 $PM_{2.5}$ filters from Magadino (Jan '13 – Sep '14), were collected over 24 h every 4th day, with a total sampled air volume of 720 m^3 per filter. Zurich-Kaserne is an urban background site, located in a courtyard in the city center of Zurich (410 meters above sea level). The location is surrounded by roads with rather low traffic and is not affected by major emissions from industries. Magadino-Cadenazzo is a rural background air quality monitoring station located in southern Switzerland, south of the Alps in the Magadino plane close to the Lago Maggiore, about two kilometers outside the small village of Cadenazzo. The site is surrounded by agricultural land and forests and is exposed to wood smoke from residential heating during winter. Biomass-burning at both sites is associated with domestic heating during winter or with open fires, agricultural waste disposal, waste burning etc., in other seasons.

S2. Measurements of aerosol size distribution and morphology

Particle (number) size distributions were measured in Zurich during 2013 using a scanning mobility particle sizer (SMPS) at 54 particle size bins between 10 to 487 nm. Data were collected continuously throughout the year with a time resolution of 10 min and averaged over 24 h every 4th day in order to have the same time resolution as the respective filter samples (sample number = 88, 3 daily samples were excluded due to instrumental issues). Volume size distributions were derived assuming spherical particles and the contribution of the different components to the mass size distributions were obtained by assuming identical particle density for all components (see Fig. S7).

A field-emission scanning electron microscope (Zeiss Supra 40 VP) coupled with an energy-dispersive X-ray spectrometer (FE-SEM-EDS) was used to observe the general morphology and deposition characteristics on the fibre filters, as well as the elemental composition of individual (non-)carbonaceous particles. The FE-SEM scanned different filter areas at magnifications up to 100000× with accelerating voltage of 5-10-20 kV, beam current value of 200 nA and work distance of 3.5 mm [secondary electrons (SE) in-lens detector]. An energy-dispersive X-ray spectrometer (EDS, Oxford Link with a Pentafet Si(Li) detector) was used to detect elements. We chose two representative winter samples, one from each site during winter with the highest BBOA contribution to OA mass.

S3. Optical measurements

S3.1: Total aerosol absorption

For both Zurich and Magadino, the total aerosol attenuation of daily samples j, $b_{\mathrm{ATN,AE33},j,i}$, was measured online at seven-wavelengths, (370, 470, 520, 590, 660, 880 and 950 nm) using a dual-spot aethalometer (AE33 model, Magee Scientific) at a time resolution of 10 min. Firmware output of loading compensation was used. In the aethalometer, light is transmitted through a particle-laden filter (I) and the effective attenuation coefficient is measured by comparing the transmission to that of a clean filter (I_0). Daily averaged $b_{\mathrm{ATN,AE33},j}(\lambda)$ were calculated, corresponding to the offline filter samples. For selected set of 27 daily offline samples (22 mm circular punches), aerosol absorption ($b_{\mathrm{abs,MWAA},j}(\lambda)$, in Mm^{-1}) was determined at five wavelengths using the multi-wavelength absorption analyser (MWAA) (Massabò et al., 2013). The MWAA measures the transmission and backward scattering at two fixed angles. Measurements were performed at 375, 407, 532, 635 and 850 nm, and power law fitting ($R^2 > 0.97$) was applied to interpolate the data to compare with the AE33 attenuation measurements. From these comparisons, wavelength-specific AE33 calibration coefficients, $C(\lambda)$, were derived using Eq. (S1):

$$C(\lambda) = \frac{b_{\mathrm{ATN,AE33},j}(\lambda)}{b_{\mathrm{abs,MWAA},j}(\lambda)} \quad \text{(S1)}$$

The mean $C(\lambda)$ values were then used to obtain from AE33 data aerosol absorption coefficients, $b_{\mathrm{abs,total},j}(\lambda)$, for the entire sample set (Eq. (S2)):

$$b_{\mathrm{abs,total},j}(\lambda) = \frac{b_{\mathrm{ATN,AE33},j}(\lambda)}{C(\lambda)} \quad \text{(S2)}$$

The 1 SD of $C(\lambda)$ variability was propagated through Eq. (S2) to obtain the respective 1 SD uncertainty in $b_{\mathrm{abs,total},j}(\lambda)$.

Similar to Corbin et al. (2019), MWAA measurements were carried out also upon extraction (using small petri dishes) of 4 Magadino 2014 and 5 Zurich 2013 $PM_{2.5}$ filters in 5 mL water and then in 5 mL methanol (1 h, 70 rpm). Results were blank-subtracted in all cases. The repeats of original or water-washed punch measurements showed very good reproducibility in the AAE values, but not always accurate in terms of absolute absorbance. This is likely due to mechanical removal of insoluble particles, as we could confirm through SEM analysis of evaporated aerosol extracts (Fig. S13). Therefore, here we used only the AAE values as a measure of the wavelength dependence of the remaining aerosol, under the assumption that particle mechanical removal with extraction is not selective to certain insoluble aerosol.

S3.2: Absorption of aerosol extracts

The experimental setup and detailed analytical protocol for absorption measurement in extracts were described in our earlier publication (see SI of Moschos et al., 2018). Briefly, attenuation spectra of aerosol extracts in ultrapure water or methanol were measured from 280 nm to 600 nm using a UV-visible spectrophotometer (Ocean Optics) coupled to long-path detection cell (length l = 50 cm). The instrument records the light attenuation in solution, $\mathrm{ATN}^{10}_{\mathrm{sol}\,j}(\lambda)$, for a sample j as a function of wavelength, as the decadic logarithm of the ratio of signal intensities of the reference (solvent, I_0) and the sample (I), both corrected for background

signals with the light source off. From $\mathrm{ATN}^{10}_{\mathrm{sol}\,j}(\lambda)$, the absorption coefficient in solution (in Mm^{-1}), $\boldsymbol{A} = \mathrm{Abs}_{\mathrm{UV-vis},j}(\lambda)$, can be quantified (Hecobian et al., 2010) based on the Lambert-Beer law (Eq. (S3)), assuming that additional light scattering by the solute can be neglected upon dissolution:

$$A_{\mathrm{j}}(\lambda) = \mathrm{Abs}_{\mathrm{UV-vis},j}(\lambda) = \frac{\mathrm{ATN}^{10}_{\mathrm{sol}\,j}(\lambda)}{l} \cdot \ln 10 \cdot \left(\frac{V_{\mathrm{sol}}}{V_{\mathrm{air}}}\right)_j \qquad \text{(S3)}$$

where V_{air} and V_{sol} are the volumes of air sampled through the filter (punch) and solvent used during the extraction (both in m^3), respectively. In this work, when the solvent was methanol, the extract volume was 3 or 6 mL and PTFE syringe filters of same dimensions (0.45 μm) were used (0.22 vs. 0.45 μm filtering did not have any noticeable effect on the recorded spectra).

S4. UV/Vis-PMF applications

We performed an exploratory analysis (Table S1) to determine which factors from each AMS-PMF solution drive the measured absorbance in methanol. This analysis was based on the correlation between the factor mass and the absorbance, for the full dataset of each factor solution, and for selected time points where each factor dominates in terms of mass compared to other absorbing fractions. The outcome of this analysis pointed to the inclusion of all OA factors in the UV/Vis-PMF model, except for SCOA and PBOA that contribute significantly to the coarse-mode (PM_{10}-$PM_{2.5}$) mass. Also, the absorbance of the coarse fraction in Magadino during 2014 contributed significantly less to PM_{10} absorbance than its respective contribution to PM_{10} mass (Fig. S8). HOA, COA, fOOA and SOOA were combined into a single (for each AMS-PMF solution) "other OA" factor before the UV/Vis-PMF analysis, because initial model runs showed that their individual contributions to absorbance were consistently lower than those of BBOA and WOOA. It was also confirmed, by considering all OA factors in the model, that the scaled residuals were not further reduced by including SCOA and PBOA (Fig. S9), which further demonstrated that these fractions did not contribute significantly to the absorbance of the PM_{10} aerosol fraction. UV/Vis-PMF (Moschos et al., 2018) was then constrained using three factors (BBOA, WOOA, other OA) and was applied to both methanol-soluble ($A_{\mathrm{MeOH},j}(\lambda)$) and water-insoluble ($A_{\mathrm{MeOH},j}(\lambda) - A_{\mathrm{H2O},j}(\lambda)$) absorbance matrices, where $A_{\mathrm{H2O},j}(\lambda)$ was corrected for the water/methanol solvent effect (Fig. S5). The application of UV/Vis-PMF on the water-insoluble absorbance data showed that, unlike BBOA, WOOA and other OA did not explain a quantifiable portion of the absorbance (too low or noisy contributions). For example, for case (g) mentioned in this section, water-insoluble BBOA could explain the totality of the input water-insoluble absorbance at 370 nm. For the calculation of $k(\lambda)$ for methanol-soluble BBOA and water-insoluble (but methanol-soluble) BBOA, we multiplied the total AMS-PMF BBOA mass with 0.93 to account for the average extraction efficiency of BBOA in methanol (Fig. S6). Also, the estimated solubility of WOOA and BBOA in water was up to 90 % and 66 %, respectively, based on the calculated recoveries by AMS-PMF analysis (Daellenbach et al., 2017; Vlachou et al., 2018). WOOA can thus be considered fully water-soluble. We examined the uncertainties in $k(\lambda)$ (or $MAE(\lambda)$) by varying the sample size of the input matrices, using the respective factor mass concentrations from the offline AMS-PMF Solutions 1 and 2. Specifically, the spatial coverage and temporal coverage or resolution were reduced compared to the full dataset runs for each PM_{10} AMS-PMF factor solution, as follows (the retrieved factor-specific *k* at 370 nm from the different sensitivity runs is shown in Table S2):

a) Solution 2: full dataset; Magadino and Zurich 2013 (182 time points)
b) Solution 2: Magadino 2013 alone (91 time points)
c) Solution 2: Zurich 2013 alone (91 time points)
d) Solution 2: first two filters per month; Magadino and Zurich 2013 (48 time points)
e) Solution 2: last two filters per month; Magadino and Zurich 2013 (48 time points)
f) Solution 1: full dataset; Magadino 2013/14 (154 time points)
g) Solution 1: Magadino 2013/14 winter (64 time points)
h) Solution 1: Magadino 2013/14 summer (90 time points)
i) Solution 1: first two filters per month; Magadino 2013/14 (42 time points)
j) Solution 1: last two filters per month; Magadino 2013/14 (42 time points)

S5. Calculation of MAC/MAE$_{370\mathrm{nm}}$

The factor contributions to particulate BrC absorption were obtained by considering the following cases for the source-specific BrC particle size and mixing states with other NR-PM (OOA = sum of the different OOA factors):

Case 1; BBOA in the smaller size range (120 nm), externally mixed with inorganics; OOA in the larger size range (200-400 nm), externally mixed with inorganics.

Case 2; BBOA in the larger size range (200-400 nm), externally mixed with inorganics; OOA in the larger size range (200-400 nm), externally mixed with inorganics.

Case 3; BBOA in the larger size range (200-400 nm), externally mixed with inorganics; OOA in the larger size range (200-400 nm), internally mixed with inorganics.

Case 4; BBOA in the smaller size range (120 nm), externally mixed with inorganics; OOA in the larger size range (200-400 nm), internally mixed with inorganics.

Case 5; BBOA + OOA + inorganics, all internally mixed in the larger size range (200-400 nm).

Case 6; BBOA in the smaller size range (120 nm), externally mixed with inorganics; OOA factors externally mixed from each other in the larger size range (200-400 nm), externally mixed with inorganics.

Case 7; BBOA in the larger size range (200-400 nm), externally mixed with inorganics; OOA factors externally mixed from each other in the larger size range (200-400 nm), externally mixed with inorganics.

We considered an OOA particle size of 200-400 nm ("larger size range") and a lower limit of ~120 nm for primary (non-OOA) BrC, based on available SMPS data for Zurich (Fig. S7). Fresh BBOA is known in certain cases to have smaller diameter, e.g. from SP2 measurements in Paris (Laborde et al., 2013). Therefore, we have considered the above cases where BBOA occurs in smaller sizes. HOA and COA were treated as externally mixed small size particles except for "case 5". Furthermore, past size distributions from Zurich (Wolf et al., 2017) indicate that (W)OOA most likely resides in the accumulation-mode. PBOA and SCOA were not considered in these cases, because these fractions reside mainly in the coarse-mode and thus are not expected to be internally mixed with other aerosol fractions.

For each case, we obtained the effective k, k_{mix}, of each particle type, p (Eq. (S4)), by using the median wavelength-dependent $k(\lambda)$ of methanol-soluble WOOA, BBOA and other OA estimated by UV/Vis-PMF, multiplied with the mass fraction (f) of each aerosol component X in the different particle mixtures (volume mixing rule). The total BBOA mass was assumed to have similar absorptivity to the methanol-soluble BBOA.

$$k_{\mathrm{mix},j}(\lambda) = \sum_X \left[\overline{k}_X(\lambda) \cdot f\{[X]_{p,j}\} \right] \quad \text{(S4)}$$

We converted the resulting $k_{\mathrm{mix},j}(\lambda)$ to mass absorption cross-sections (MAC) at four AE33 wavelengths (370 nm, 470 nm, 520 nm, 590 nm) with Mie code programmed in the software package Igor Pro (WaveMetrics). The resulting mass absorption cross-sections of each particle type, $\mathrm{MAC}_j(p,\lambda)$, were multiplied with the total mass concentrations of its constituents to obtain the respective absorption coefficients, $b_{\mathrm{abs}}{}^{\mathrm{BrC-p}}_{\mathrm{Mie},j}(\lambda)$, at the different AE33 wavelengths, using Eq. (S5):

$$b_{\mathrm{abs}}{}^{\mathrm{BrC}-p}_{\mathrm{Mie},j}(\lambda) = [X]_{p,j} \cdot \mathrm{MAC}_j(p,\lambda) \quad \text{(S5)}$$

The retrieved $b_{\mathrm{abs}}{}^{\mathrm{BrC}-p}_{\mathrm{Mie},j}(\lambda)$ values for each particle type were summed to obtain the total absorption coefficient from all BrC-containing particles, $b_{\mathrm{abs,BrC-Mie},j}(\lambda)$ for each sample and each of the seven cases, using Eq. (S6):

$$b_{\mathrm{abs,BrC-Mie},j}(\lambda) = \sum_p b_{\mathrm{abs,BrC-Mie},j}(p,\lambda) \quad \text{(S6)}$$

The factor-specific and total BrC MAC/MAE values at 370 nm from the seven distinct mixing state cases are summarised in Table S3. The calculations for total MeOH-BrC (last column) were based on the following notation: $b_{\mathrm{abs,BrC-Mie}} = (\mathrm{MAC}/\mathrm{MAE})_{\mathrm{NR-PM}} * \mathrm{MAE}_{\mathrm{totalOA}} * [\mathrm{OA}]$, where $\mathrm{MAE}_{\mathrm{NR-PM}} * [\mathrm{NR-PM}] = \mathrm{MAE}_{\mathrm{totalOA}} * [\mathrm{OA}]$. The MAC/MAE uncertainty corresponds to the full range between the min. and max. total BrC absorption values from the seven cases.

SUPPORTING TABLES AND FIGURES

Table S1. Exploratory analysis for AMS-PMF factor selection in the UV/Vis-PMF model. The individual factors eventually considered to constrain the model were based on specific correlation criteria; no fully transparent OA fractions were included in the model, i.e. R^2 between factor mass time series and bulk methanol solution absorbance (PM_{10} or coarse) time series < 0.4, for selected time points where each OA factor (PM_{10} or coarse) mass dominates compared to that of other absorbing factors (coarse data existed only for data from 2014, so the correlations with the coarse fraction could be tested only for Solution 1; only positive values for both the coarse fraction mass and absorbance were used). Note that the Pearson's *r* was positive in all cases except for the coarse PBOA (the respective R^2 value are indicated with an asterisk).

Factor	**Mass ratio criterion**	**Number of time points**	**R^2; Factor mass vs. bulk absorbance time series**
AMS-PMF «Solution 2»			
BBOA	(Block)	182	0.92
	BBOA:WOOA>3	27	**0.98**
	WOOA:BBOA>3	42	0.75
	SOOA:(BBOA+WOOA)>3	32	0.36
WOOA	(Block)	182	0.36
	WOOA:BBOA>3	42	**0.83**
	BBOA:WOOA>3	27	0.80
	SOOA:(BBOA+WOOA)>3	32	0.38
SOOA	(Block)	182	0.06
	SOOA:(BBOA+WOOA)>3	32	**0.56**
HOA	(Block)	182	0.17
	HOA:(BBOA+WOOA)>1	29	**0.71**
COA	(Block)	182	0.12
	COA:(BBOA+WOOA)>1	25	**0.78**
SCOA	(Block)	182	0.17
	SCOA:(BBOA+WOOA)>1	39	0.37
AMS-PMF «Solution 1»			
BBOA	(Block)	154	0.90
	BBOA:WOOA>3	59	**0.93**
	WOOA:BBOA>3	27	0.79
	SOOA:(BBOA+WOOA)>3	55	0.24
WOOA	(Block)	154	0.21
	WOOA:BBOA>3	27	**0.96**
	BBOA:WOOA>3	59	0.30
	SOOA:(BBOA+WOOA)>3	55	0.44
SOOA	(Block)	154	0.25
	SOOA:(BBOA+WOOA)>3	55	**0.54**
HOA	(Block)	154	0.22
	HOA:(BBOA+WOOA)>1	25	**0.45**
fOOA	(Block)	154	0.05
	fOOA:(BBOA+WOOA)>2	37	**0.42**
SCOA	(Block)	154	0.09
	SCOA:(BBOA+WOOA)>1	21	0.00
PBOA	(Block)	154	0.06
	PBOA:(BBOA+WOOA)>4	34	0.17
SCOA (coarse)	(Block)	154	0.11
PBOA (coarse)	(Block)	154	0.30*

Table S2. UV/Vis-PMF-based *k* of the methanol-soluble BrC factors at 370 nm from different sensitivity runs.

k_{370nm}	BBOA	WOOA	Other OA	WINS-BBOA
a	0.067	0.025	0.0064	0.075
b	0.070	0.024	0.0010	0.082
c	0.078	0.030	0.0057	0.127
d	0.067	0.030	0.0057	0.094
e	0.069	0.025	0.0077	0.083
f	0.046	0.038	0.0043	0.039
g	0.046	0.041	0.0046	0.042
h	0.058	0.041	0.0026	0.063
i	0.045	0.031	0.0079	0.045
j	0.046	0.025	0.0080	0.044
1st quartile	0.046	0.025	0.0044	0.044
median	0.062	0.030	0.0057	0.069
3rd quartile	0.068	0.036	0.0074	0.083

Table S3. Factor-specific and total BrC MAC/MAE at 370 nm obtained for seven distinct mixing state cases through Eq. (S4). The "±" sign indicates the day-to-day variability for all 245 PM_{10} filter samples from Magadino and Zurich. The full-dataset MAC/MAE for HOA, COA, SOOA and fOOA was calculated using the UV/Vis-PMF output median *k* of the combined "other OA" factor (Fig. 2) and each factor mass from the respective AMS-PMF factor solution. Note that for "case 5" (fully internally mixed BBOA + OOA + inorganics), the conversion factor is identical for all absorbing AMS-PMF source components. The min. and max. (from the seven cases) MAC/MAE were used to convert the UV/Vis-PMF-based median *k* (Fig. 2) to factor-specific particulate MAC values [min, max] in the last row, considering the MAC/MAE uncertainty.

MAC:MAE @ 370 nm	BBOA	WOOA	Other OA (combined)	HOA	COA	SOOA	fOOA	**Total MeOH-BrC**
Case 1	1.05	1.66 ± 0.04	1.48 ± 0.17	1.09	1.09	1.66 ± 0.04	1.68 ± 0.03	1.33 ± 0.16
Case 2	1.35	1.66 ± 0.04	1.48 ± 0.17	1.09	1.09	1.66 ± 0.04	1.68 ± 0.03	1.48 ± 0.08
Case 3	1.35	1.71 ± 0.02	1.51 ± 0.17	1.09	1.09	1.71 ± 0.02	1.71 ± 0.02	1.50 ± 0.09
Case 4	1.05	1.71 ± 0.02	1.51 ± 0.17	1.09	1.09	1.71 ± 0.02	1.71 ± 0.02	1.35 ± 0.17
Case 5	1.60 ± 0.12							
Case 6	1.05	1.55	1.51 ± 0.17	1.09	1.09	1.71	1.71	1.31 ± 0.15
Case 7	1.35	1.55	1.51 ± 0.17	1.09	1.09	1.71	1.71	1.46 ± 0.07
(min+max)/2	*1.33 ± 0.06*	*1.61 ± 0.04*	*1.55 ± 0.09*	*~1.35*	*~1.35*	*~1.66*	*~1.66*	*~1.45*
MAC_{370nm} ($m^2\ g^{-1}$)	*[1.48, 2.26]*	*[1.05, 1.16]*	*~0.20*					

Table S4. Different proxy results tested for the determination of bare BC MAC at 660 nm for three different cases, following a stepwise multiple linear regression approach. Only data points in the linear proxy (NR-PM:EC) range were considered for the linear fits. (OOA+BBOA+m-SIA):EC was the most consistent of the tested proxies for the three cases, in terms of the obtained MAC for bare BC, slope and Pearson's *r*, indicating that OOA, BBOA and inorganics likely partitioned to coatings on EC leading to its absorption enhancement by acting as a lens.

NR-PM	**MAC_{bareBC}** (intercept)	**Slope**	**Pearson's *r***
Magadino 2013/14 winter			
OA	5.68 ± 0.78	0.413 ± 0.059	0.67
OA+m-SIA	6.37 ± 0.52	0.236 ± 0.025	0.78
OOA	7.32 ± 0.50	0.741 ± 0.099	0.70
OOA+m-SIA	8.07 ± 0.41	0.231 ± 0.028	0.73
OOA+BBOA+HOA+m-SIA	6.61 ± 0.46	0.240 ± 0.020	0.79
OOA+BBOA+m-SIA	6.54 ± 0.47	0.261 ± 0.026	0.79
Magadino 2013/14 summer			
OA	5.49 ± 0.89	0.258 ± 0.058	0.44
OA+m-SIA	5.64 ± 0.95	0.194 ± 0.048	0.41
OOA	6.26 ± 0.53	0.322 ± 0.051	0.56
OOA+m-SIA	6.21 ± 0.67	0.219 ± 0.045	0.47
OOA+BBOA+HOA+m-SIA	5.79 ± 0.73	0.231 ± 0.046	0.49
OOA+BBOA+m-SIA	5.91 ± 0.70	0.229 ± 0.046	0.49
Zurich 2013			
OA	6.46 ± 0.66	0.398 ± 0.064	0.55
OA+m-SIA	6.11 ± 0.35	0.205 ± 0.016	0.81
OOA	8.14 ± 0.45	0.436 ± 0.070	0.51
OOA+m-SIA	6.84 ± 0.32	0.226 ± 0.020	0.78
OOA+BBOA+HOA+m-SIA	6.58 ± 0.30	0.211 ± 0.015	0.82
OOA+BBOA+m-SIA	6.76 ± 0.30	0.216 ± 0.017	0.81

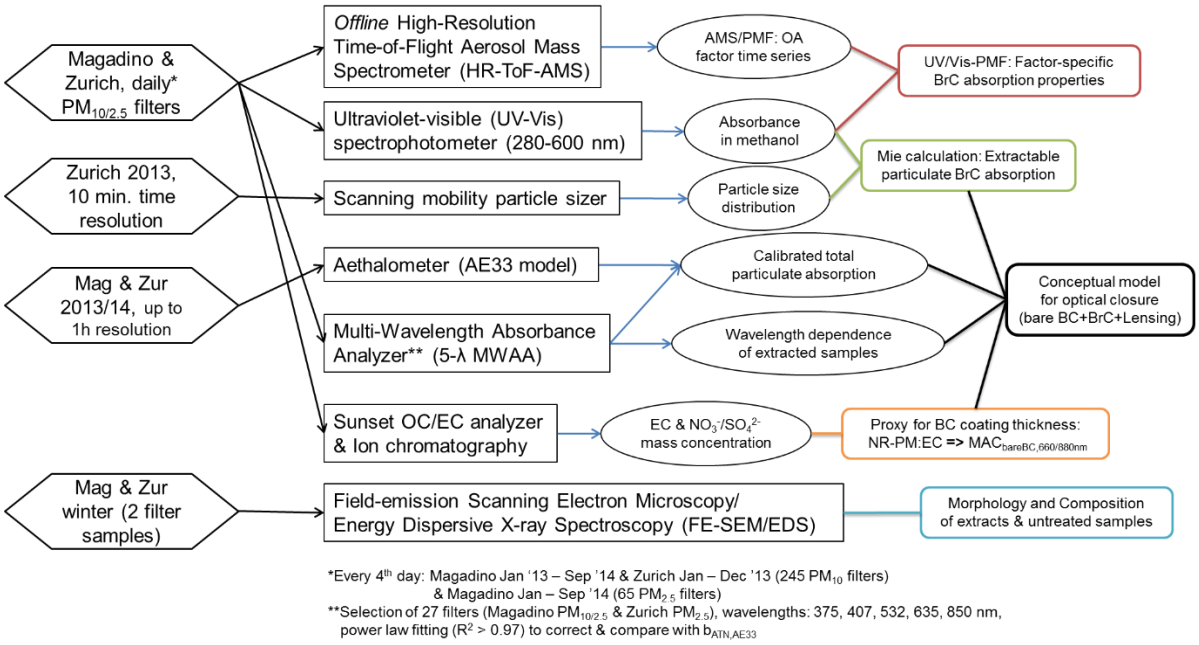

Figure S1. Flowsheet of how to obtain the various (mass) absorption coefficients, EC mass concentration and other aerosol properties from the raw filter-based data delivered by different types of instruments and methods. These were then used to obtain multi-wavelength optical closure for the different absorbing species.

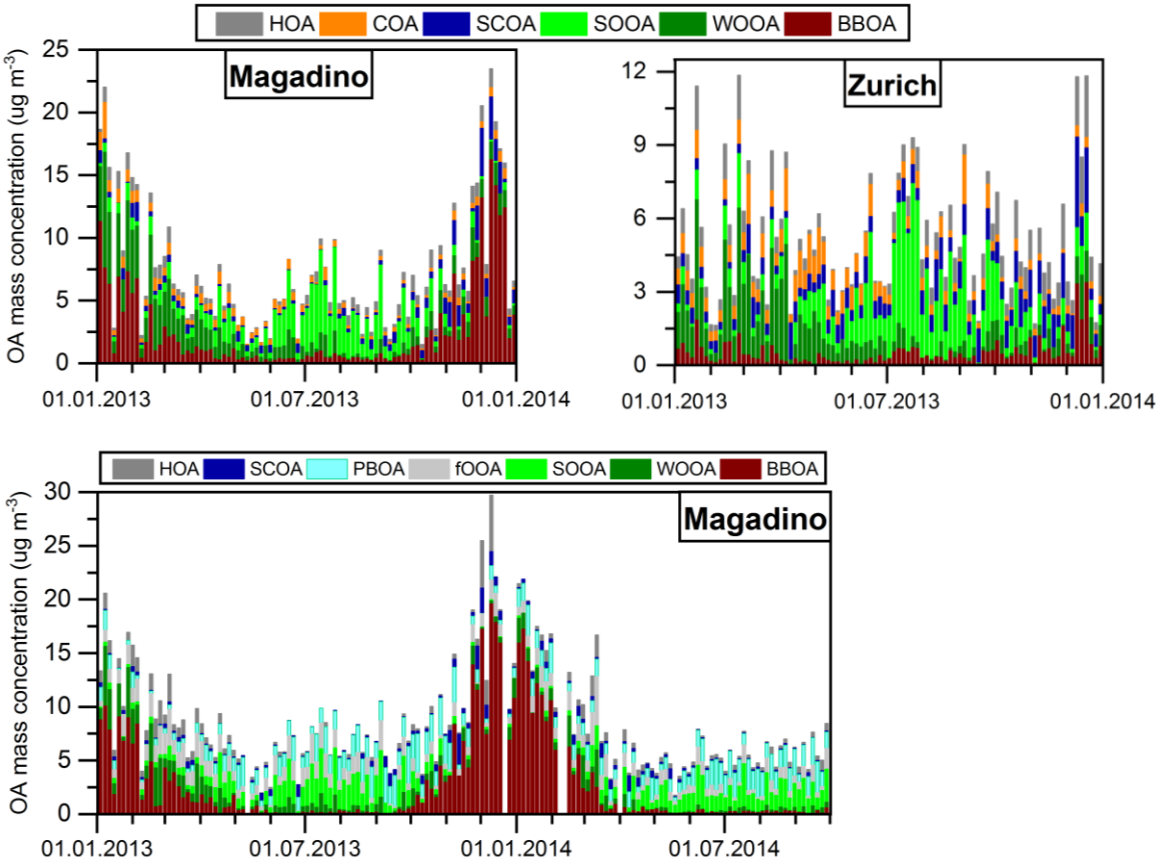

Figure S2. Time series of offline PM_{10} total OA (by applying source-specific recoveries) AMS-PMF factors (Sect. S2). Upper panels: Solution 2 (Daellenbach et al., 2017); Lower panel: Solution 1 (Vlachou et al., 2018), used as constraints in UV/Vis-PMF (Sect. 2.2). Note the non-negligible WOOA mass in spring and summer and the important contribution of BBOA in Magadino during winter and in Zurich in November-December 2013.

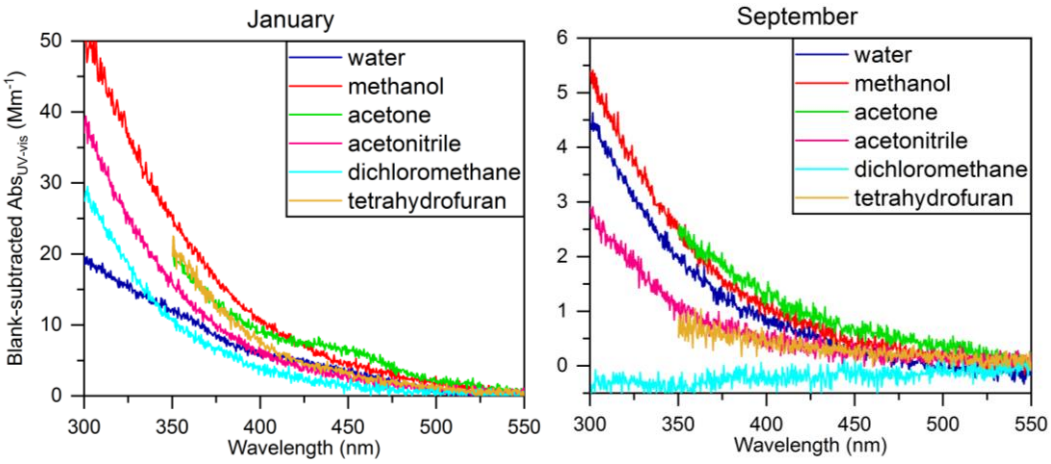

Figure S3. Calculated absorbance for a winter and summer filter extracted in different solvents. Acetone and acetonitrile have a larger dipole moment than methanol, no hydrogen bonds and can dissolve charged species. An absorption hump around 470 nm was observed at longer wavelengths for water and acetone. Acetone, which is less polar than methanol, provided comparable results but had the disadvantage of a cut-off wavelength of 330 nm, whereas the absorbance in water was significantly lower than in methanol for the Magadino winter sample. The absorbance in dichloromethane (the least polar of the tested solvents) was negligible for the summer sample. Methanol was selected in this study for optical closure purposes considering the obtained absorbance in the full wavelength range, as well as the extraction efficiency of BBOA-dominated samples in methanol (Fig. S6).

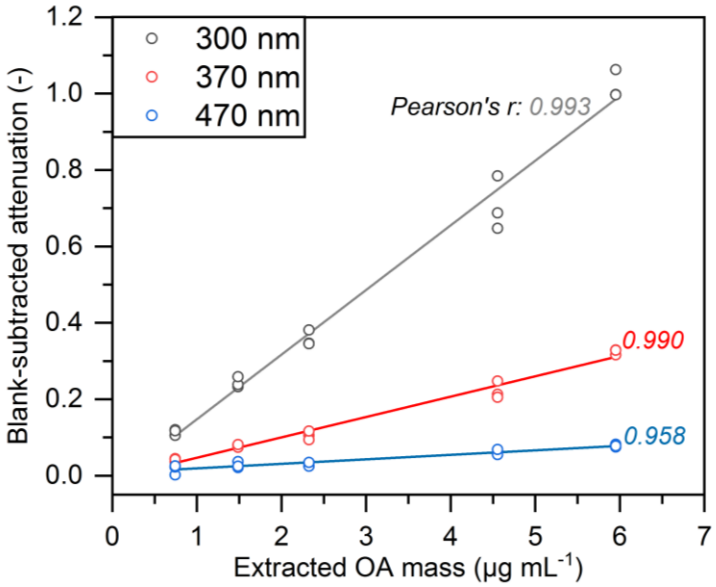

Figure S4. Linearity of ATN_{sol}^{10} obtained at three different wavelengths for a Magadino 2014 $PM_{2.5}$ filter sample extracted in methanol three times at five different concentrations, covering the full range of our solvent extraction (*x* axis) and UV-vis measurement (*y* axis) conditions.

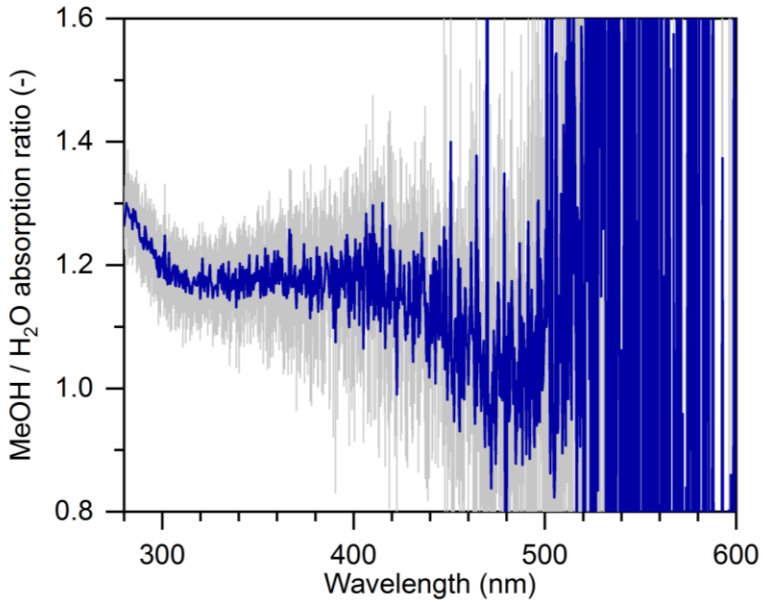

Figure S5. Assessment of the water vs. methanol solvent effect on UV-vis measurements, performed by comparing the attenuation spectra for ambient PM extracted in water and then diluted in methanol or in water in a 10/90 ratio. The blue curve and grey shading indicate the average and 1 SD, respectively, from 5 Magadino 2014 $PM_{2.5}$ samples. The ratio at 280-470 nm was higher than that calculated in previous study (Phillips and Smith, 2017), whereas above 470 nm we considered a ratio of 1.0 because the signal was noisy. The water-insoluble (but methanol-soluble) BrC absorbance used in UV/Vis-PMF, $\boldsymbol{A_{MeOHonly} = A_{MeOH} - A_{H2O}}$, was corrected for the solvent effect by multiplying $\boldsymbol{A_{H2O}}$ with the average wavelength-dependent absorption ratio below 470 nm.

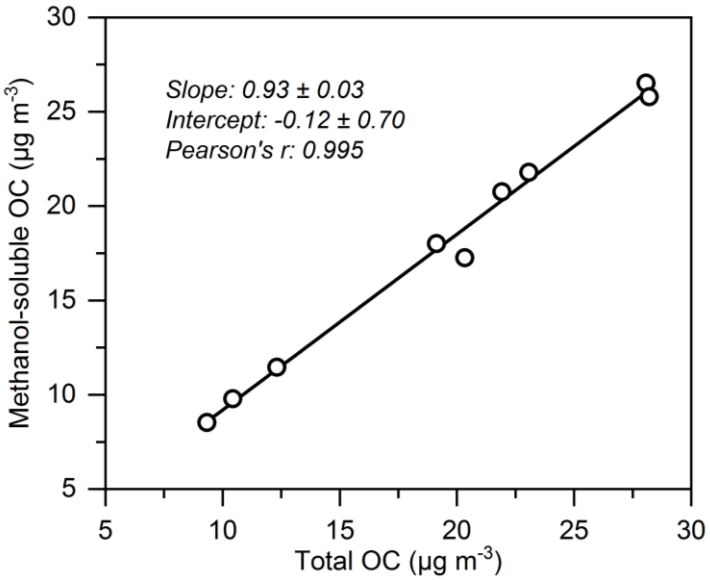

Figure S6. Estimation of BBOA extraction efficiency in methanol, determined from Sunset measurements (EUSAAR2 protocol) of untreated (*x* axis) and methanol-extracted PM_{10} filter samples from Magadino 2014 and San Vittore (rural) 2013 (November, December and January) with maximum contribution of BBOA to total OA mass. The $k_{(WINS-)BBOA}$ were corrected for the (minimum) extraction efficiency (93 ± 3 %), by multiplying the total BBOA mass with 0.93 (Text S4).

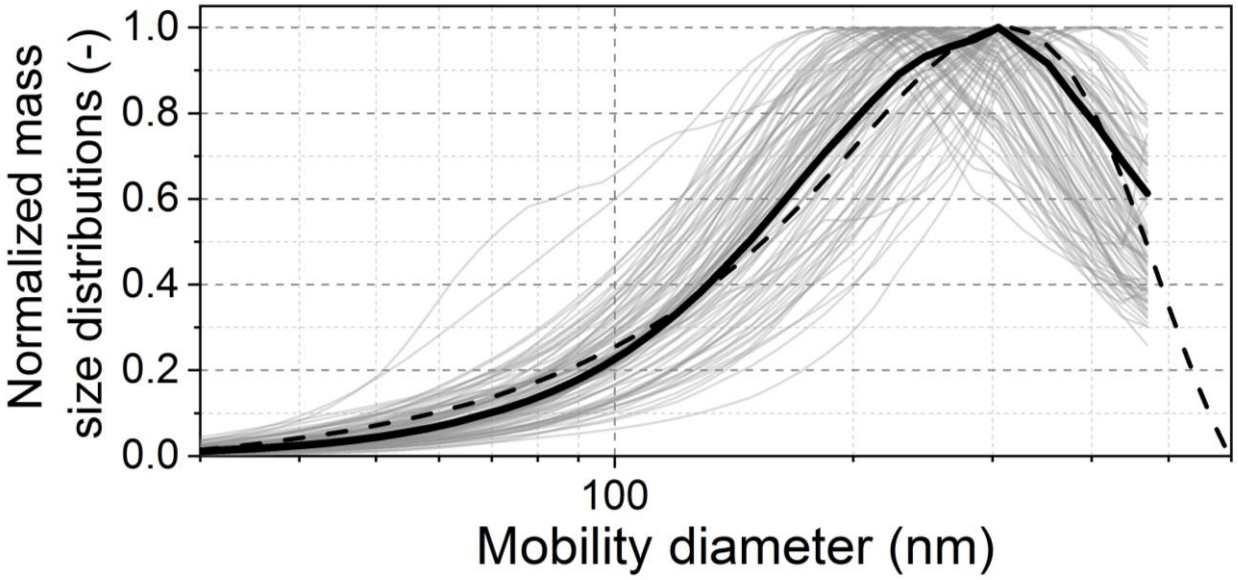

Figure S7. Normalised mass size distributions based on year-long SMPS measurements in Zurich during 2013. Thin grey lines are daily averaged distributions that match the time resolution of the collected filters. The thick black line shows the yearly average distribution, extrapolated with the dashed line assuming a log-normal distribution.

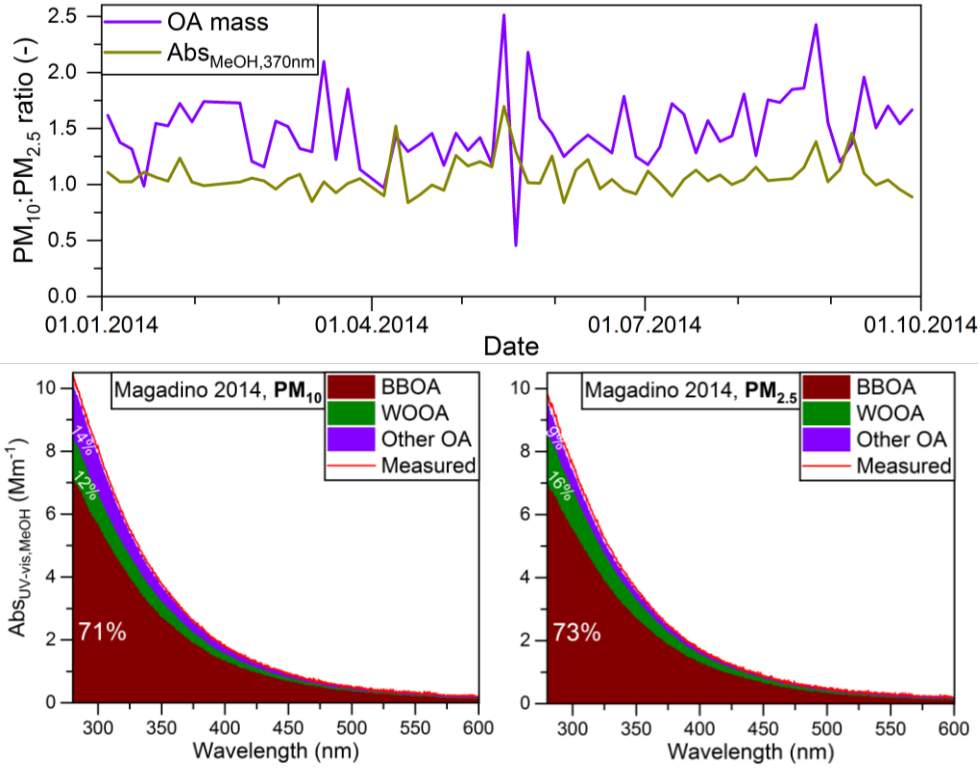

Figure S8. Upper panel: the coarse (PM_{10}-$PM_{2.5}$) fraction of the aerosol is a negligible contributor to overall absorbance (~5 %) despite its significant contribution to PM_{10} mass. Lower panels: UV/Vis-PMF output for Magadino 2014 (Jan-Sep) where both $PM_{2.5}$ and PM_{10} data existed for both AMS-PMF factor mass and UV-vis absorbance, with all 7 factors being used here as model constraints. The model apportioned the absorbance of the two size fractions predominantly and consistently to BBOA and WOOA. The red line shows the measured absorbance (unexplained absorbance ~2-3 %).

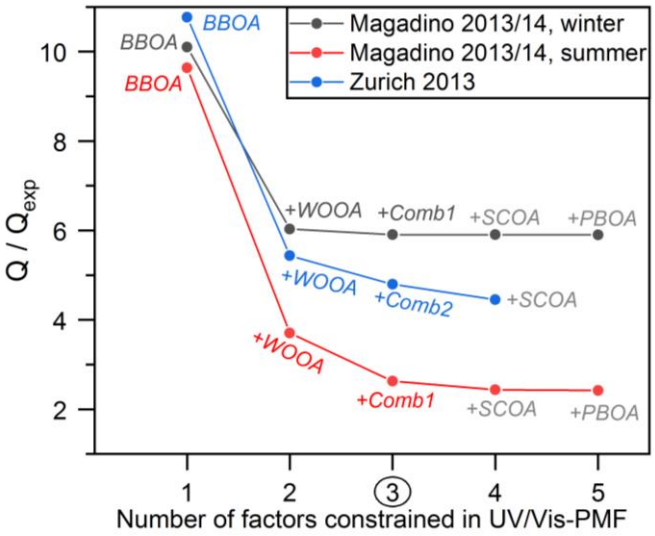

Figure S9. Reduction of scaled residuals (Q/Q_{exp}) with increasing number of factors constrained in UV/Vis-PMF, clearly showing that BBOA alone did not explain the variability in the measured absorbance. Comb2: SOOA+HOA+COA (AMS-PMF Solution 2); Comb1: SOOA+HOA+AOOA (AMS-PMF Solution 1). BBOA, WOOA and Comb (or "other OA") were used as model constraints, considering also the correlation analysis shown in Table S1. The Q/Q_{exp} values for the 3-factor (BBOA, WOOA, Comb) solutions were 5.9, 2.6 and 4.8 for Magadino winter, Magadino summer and Zurich, respectively.

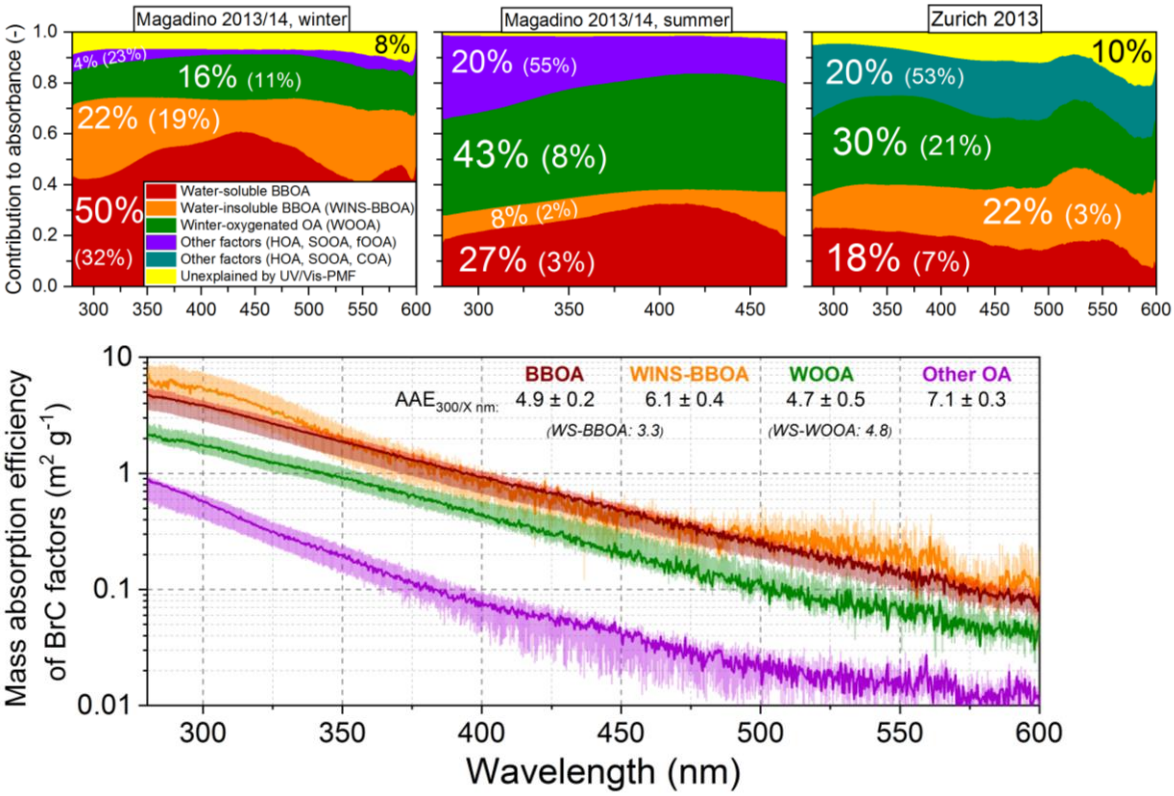

Figure S10. Upper panels: highly spectrally resolved cumulative relative contributions to absorbance of methanol-extracted PM_{10} aerosol, apportioned by UV/Vis-PMF analysis (Moschos et al., 2018) to various OA source components resolved by offline aerosol mass spectrometry (Fig. S2), demonstrated for three different model runs. Data were smoothed for demonstration, whereas summer data above 470 nm are highly uncertain (low absorbance). Labels show the contributions to absorbance averaged across the entire wavelength range, whereas the absorbing (model input) factor contributions to OA mass are shown in parentheses. Lower panel: absorption properties (AAE, median MAE and IQR) of the methanol-soluble BrC sources obtained by UV/Vis-PMF, based on sensitivity runs (Text S4, Table S2) including the three case studies shown in the upper panels, and their comparison to the water-soluble (WS) BrC factor AAEs (Moschos et al., 2018).

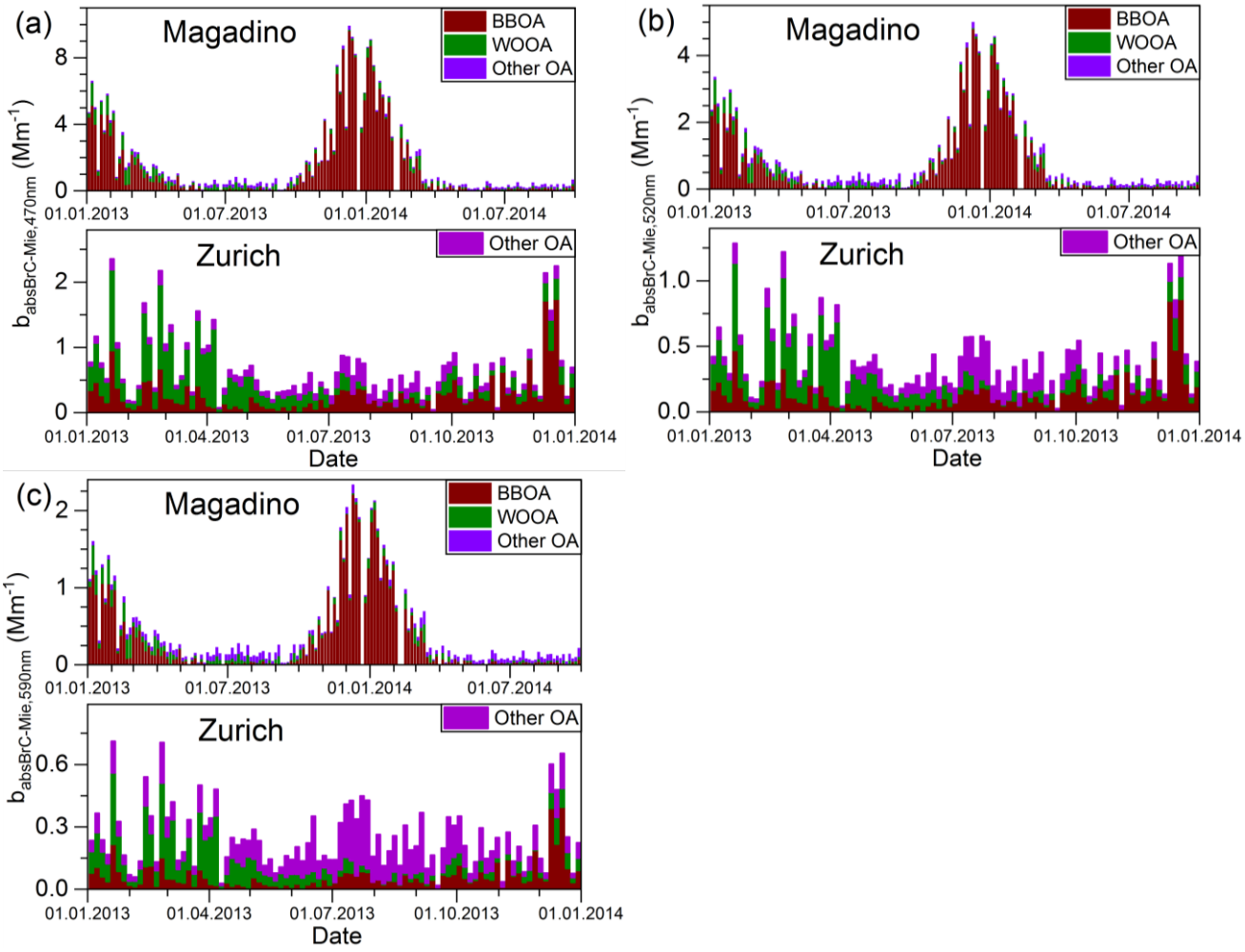

Figure S11. Time series of the average cumulative BBOA, WOOA and other OA factor contributions to Mie-predicted particulate BrC absorption at 470 nm (a), 520 nm (b) and 590 nm (c) for Magadino and Zurich.

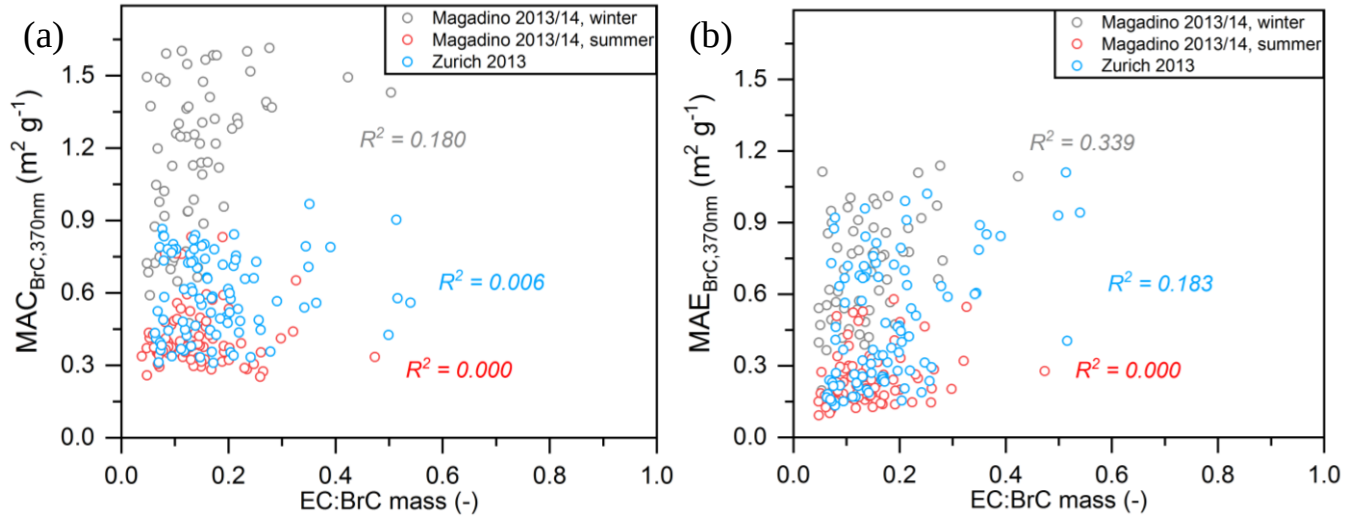

Figure S12. a) Correlation between the average time resolved $MAC_{BrC,370nm}$ and the EC-to-BrC mass ratio for ambient filter samples from Magadino and Zurich in both seasons. BrC is considered as the total OA without the contributions of the non-absorbing SCOA and PBOA (i.e. BBOA + WOOA + other OA). No significant trend is observed, which limits the applicability of the respective parameterisation (Saleh et al., 2014) to ambient (mixed-source, aged and processed) samples. b) Same as (a) but with MAE values.

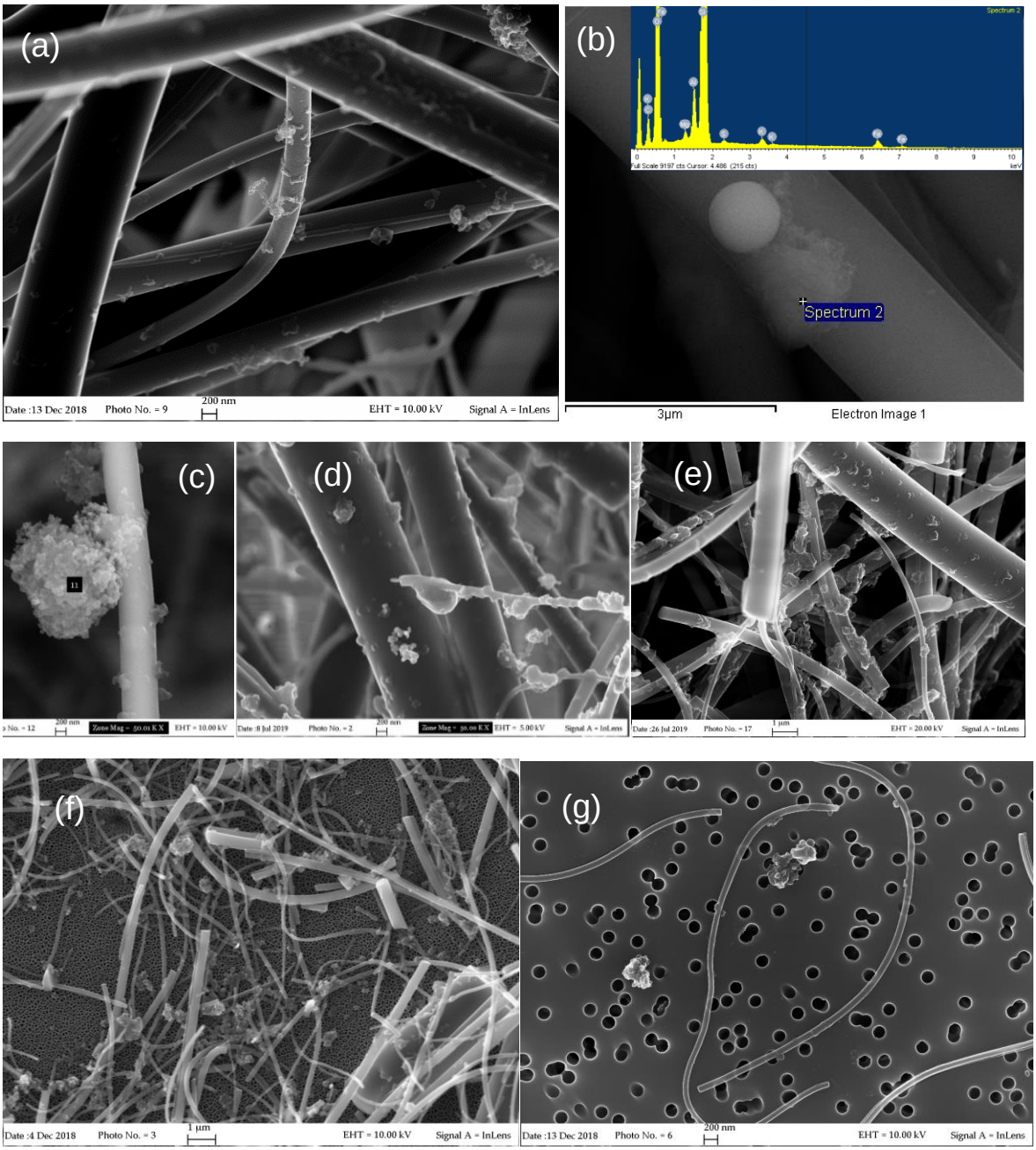

Figure S13. FE-SEM-EDS images of selected untreated filters from Zurich (a and b) and Magadino (c and d) winter. Carbon assemblies exhibit scarce adhesion onto the filter fibres and accumulate onto deeper, thinner and rougher fibres and their intersections (a). While the only spherical particles observed in untreated Zurich samples were non-carbonaceous, either Fe-bearing or containing K, Mg, Ca, Al and S (b), in Magadino both bare -including both lacey and compact/collapsed- BC (c) and drop-shape bigger pseudo-spherical (likely deformed upon collection on the filter) (d) carbonaceous particles (with traces of K and S, based on EDS analysis) were observed, the latter disappearing after washing with water (e; in-depth magnified view), as observed in many different fields. Note that most of the organic particles/coatings, especially the more volatile ones, have not survived under vacuum and thus are not observable with this technique. f) Alumina filter (Anodisc 25 Whatman, pore size 0.1 µm), on which the supernatant was deposited after sonication of the original quartz microfibre filter in water (conditions: carbon coated, high vacuum; voltage: 10 kV, signal: SE in-lens), and g) polycarbonate filter (isopore membrane track-etched, pore size 0.2 µm), on which the supernatant was filtered after water washing of the original quartz filter, showing that the washing with water seemed to remove (mechanically) a noticeable quantity of carbon nanoparticle aggregates, whereas quartz fibres were also detached.

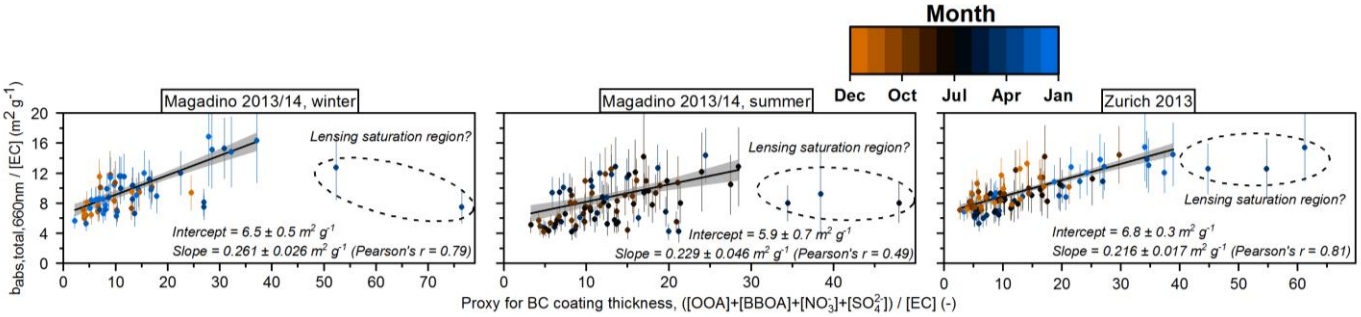

Figure S14. Calculation of MAC_{bareBC} as the intercept of uncertainty-weighted linear fits (95 % confidence interval for the slope and intercept shown) of $MAC_{BC,660nm}$ vs. the selected proxy for BC coating thickness, upon obtaining no significant evidence of a source-dependent MAC_{BC} (Fig. 4b).

REFERENCES

Corbin, J. C., Czech, H., Massabò, D., de Mongeot, F. B., Jakobi, G., Liu, F., Lobo, P., Mennucci, C., Mensah, A. A., Orasche, J., Pieber, S. M., Prévôt, A. S. H., Stengel, B., Tay, L. L., Zanatta, M., Zimmermann, R., El Haddad, I., and Gysel, M.: Infrared-absorbing carbonaceous tar can dominate light absorption by marine-engine exhaust, npj Clim. Atmos. Sci., 2, 10.1038/s41612-019-0069-5, 2019.

Daellenbach, K. R., Stefenelli, G., Bozzetti, C., Vlachou, A., Fermo, P., Gonzalez, R., Piazzalunga, A., Colombi, C., Canonaco, F., Hueglin, C., Kasper-Giebl, A., Jaffrezo, J.-L., Bianchi, F., Slowik, J. G., Baltensperger, U., El-Haddad, I., and Prévôt, A. S. H.: Long-term chemical analysis and organic aerosol source apportionment at nine sites in central Europe: Source identification and uncertainty assessment, Atmos. Chem. Phys., 17, 13265-13282, 10.5194/acp-17-13265-2017, 2017.

Hecobian, A., Zhang, X., Zheng, M., Frank, N., Edgerton, E. S., and Weber, R. J.: Water-soluble organic aerosol material and the light-absorption characteristics of aqueous extracts measured over the southeastern United States, Atmos. Chem. Phys., 10, 5965-5977, 10.5194/acp-10-5965-2010, 2010.

Laborde, M., Crippa, M., Tritscher, T., Jurányi, Z., Decarlo, P. F., Temime-Roussel, B., Marchand, N., Eckhardt, S., Stohl, A., Baltensperger, U., Prévôt, A. S. H., Weingartner, E., and Gysel, M.: Black carbon physical properties and mixing state in the European megacity Paris, Atmos. Chem. Phys., 13, 5831–5856, https://doi.org/10.5194/acp-13-5831-2013, 2013.

Massabò, D., Bernardoni, V., Bove, M. C., Brunengo, A., Cuccia, E., Piazzalunga, A., Prati, P., Valli, G., and Vecchi, R.: A multi-wavelength optical set-up for the characterisation of carbonaceous particulate matter, J. Aerosol Sci., 60, 34-46, 10.1016/j.jaerosci.2013.02.006, 2013.

Moschos, V., Kumar, N. K., Daellenbach, K. R., Baltensperger, U., Prévôt, A. S. H., and El Haddad, I.: Source apportionment of brown carbon absorption by coupling ultraviolet–visible spectroscopy with aerosol mass spectrometry, Environ. Sci. Technol. Lett., 5, 302-308, 10.1021/acs.estlett.8b00118, 2018.

Phillips, S. M., and Smith, G. D.: Spectroscopic comparison of water- and methanol-soluble brown carbon particulate matter, Aerosol Sci. Technol., 51, 1113-1121, 10.1080/02786826.2017.1334109, 2017.

Saleh, R., Robinson, E. S., Tkacik, D. S., Ahern, A. T., Liu, S., Aiken, A. C., Sullivan, R. C., Presto, A. A., Dubey, M. K., Yokelson, R. J., Donahue, N. M., and Robinson, A. L.: Brownness of organics in aerosols from biomass-burning linked to their black carbon content, Nat. Geosci., 7, 647-650, 10.1038/ngeo2220, 2014.

Vlachou, A., Daellenbach, K. R., Bozzetti, C., Chazeau, B., Salazar, G. A., Szidat, S., Jaffrezo, J.-L., Hueglin, C., Baltensperger, U., Haddad, I. E., and Prévôt, A. S. H.: Advanced source apportionment of carbonaceous aerosols by coupling offline AMS and radiocarbon size-segregated measurements over a nearly 2-year period, Atmos. Chem. Phys., 18, 6187-6206, 10.5194/acp-18-6187-2018, 2018.

Wolf, R., El-Haddad, I., Slowik, J. G., Dällenbach, K., Bruns, E., Vasilescu, J., Baltensperger, U., and Prévôt, A. S. H.: Contribution of bacteria-like particles to $PM_{2.5}$ aerosol in urban and rural environments, Atmos. Environ., 160, 97-106, 10.1016/j.atmosenv.2017.04.001, 2017.